Oil Shale, 2023, Vol. 40, No. 4, pp. 261–282
doi: https://doi.org/10.3176/oil.2023.4.01
ISSN 0208-189X

Geochemistry of marine black shale of the Cambrian Qiongzhusi Formation, Yangtze Plate, SW China: implications for provenance and paleoweathering

Zexin Fang, Ling Guo*, Jianni Liu*

State Key Laboratory of Continental Dynamics/Northwest University, Xi'an 710069, China

Received 7 February 2023, accepted 13 October 2023, available online 10 November 2023

Abstract. *Marine black shale in the Lower Cambrian Qiongzhusi (QZS) Formation in the southwestern Yangtze Plate, SW China, is the key target for shale gas development. The paleoenvironment plays an important role in the formation of organic-rich shale. Based on the analysis of major, trace and rare earth elements (REE), the authors discussed element composition, paleoweathering and provenance of Qiongzhusi black shale (QZS shale). The results show that the main components of the Qiongzhusi Formation sample are SiO_2, Al_2O_3 and total Fe_2O_3 (TFe_2O_3), with the average values of 64.08 wt%, 15.00 wt% and 5.39 wt%, respectively. Redox-sensitive elements, such as V, Cr, Ni, Zn and U, are richer in QZS shale compared to the upper continental crust (UCC). The total concentration of REE (∑REE) of QZS shale is 174.58 ppm on average, which is higher than that of UCC (average 146.37 ppm) and the North American Shale Composite (NASC) (average 173.21 ppm). The ratios of $w(SiO_2)/w(Al_2O_3)$ and $w(Al_2O_3)/w(TiO_2)$, the Zr-TiO_2 diagram, the Th/Sc vs Zr/Sc plot, the discriminant function of F1 vs F2 and F3 vs F4, as well as the discrimination diagram of ∑REE vs La/Yb indicated that the main provenances of QZS shale are sedimentary and felsic igneous rocks. The values of a chemical weathering index, the chemical index of alteration (CIA), of the Lower QZS Formation (Stage 1) range from 51.84 to 64.33, indicating a low degree of chemical weathering and a cold and dry climate. The CIA values of the Upper QZS Formation (Stage 2) range from 66.58 to 82.42, being indicative of a medium degree of chemical weathering, probably in a humid climate.*

Keywords: *black shale, trace elements, rare earth elements, Lower Cambrian, provenance, paleoweathering.*

* Corresponding authors: e-mails *lguogeology@163.com; eliljn@nwu.edu.cn*

1. Introduction

Ediacaran to Early Cambrian (E-C transition) is considered an important interval in the Earth's history recording the explosive radiations of metazoans known as the "Cambrian explosion" [1–3]. E-C transition is marked by numerous geological events such as continental reorganization [4], post-snowball glaciers melting and sea level rise [5], and global accumulation of organic-rich shale [6–8]. Lower Cambrian strata in South China are considered critical sources of shale gas, phosphate and several metals with economic value [9]. Early Cambrian sedimentary sequences in South China are stratigraphically continuous, providing an excellent opportunity for the establishment of high-resolution chronostratigraphy [10] as well as high-resolution reconstruction of paleoenvironmental conditions. Trace elements, rare earth elements (REE) and major elements have been extensively used for assessing depositional environments for shales [11–13]. The geochemistry of shales, especially their trace element composition, is considered to represent the average composition of the upper continental crust (UCC) compared to other sedimentary rocks [14], and shales are believed to have preserved the original signature of provenance and the diagenetic history [15]. Therefore, the geochemical composition of clastic sediments has been successfully used to infer the source-area weathering conditions and provenance [16–18].

Zhang [19] studied the mineralogical characteristics of Huize black shales of the Lower Cambrian Qiongzhusi (QZS) Formation in South China and ascertained a shallow shelf depositional setting characterized by hypoxia and a reducing and hot water environment. Cheng [20] shows that the source material of the QZS Formation was generally unweathered, so it can be used as paleoenvironmental information. In addition, it was found that the lower part of the QZS Formation experienced a short oxidation event during the deposition of argillaceous limestone and silty dolomite, whereas its middle and upper parts encountered a short sulfurization environment when depositing carbonaceous shale. Fang [21] described two sedimentary subfacies and established that there were two transgression and regression cycles during the deposition of QZS black shale (QZS shale) and that the seawater column was in an anoxic-sulfidic state as a whole. Cheng [22] analyzed black shale's metal-ore potential aspects using ore-forming element enrichment coefficients, late superposition intensity and ore-forming element variation coefficients. However, previous investigations focused mainly on the paleogeography, sedimentary facies and sedimentary environment of the study area and the formation relationship between black shale series and various metal-nonmetal deposits.

In the current study, the sedimentary geochemistry of Early Cambrian QZS Formation organic-rich shales in the southwestern Yangtze Plate, SW China was investigated. The main aims of the current research were: 1) to obtain refined geochemical data to reveal the short- and long-term paleoenvironmental

forcing on the Early Cambrian black shale sedimentation; 2) to reconstruct the black shale's provenance; and 3) to elucidate the variations in the chemical weathering intensity of the Early Cambrian, southwestern Yangtze Plate, SW China.

2. Geologic setting

The study area is located on the Upper Yangtze Plate, SW China (Fig. 1a). In the Early Cambrian (~520 Ma), the Yangtze Plate was situated in the equatorial position as an isolated island near the Western Gondwana Coast [23]. During the development of the QZS Formation, the Yangtze Plate submerged and a sandy-muddy shelf formed in Middle Stage 2 to Middle Stage 3 (Meishucunian-Qiongzhusian Stages, ~526 to ~515 Ma) because of large-scale transgression (Fig. 1b).

The Lower Cambrian succession of the Upper Yangtze Plate consists of the Yuhucun Formation, the QZS Formation and the Canglangpu Formation (Fig. 1c). The Yuhucun Formation is mainly composed of dolomite, siliceous rock, phosphorite and limestone. The QZS Formation is chiefly gray-black fine-grained siltstone, while its upper part is made of dark-gray shale and mudstone mixed with siltstone with trilobite fossils, fine sandstone and a small amount of limestone. The Canglangpu Formation can be divided into

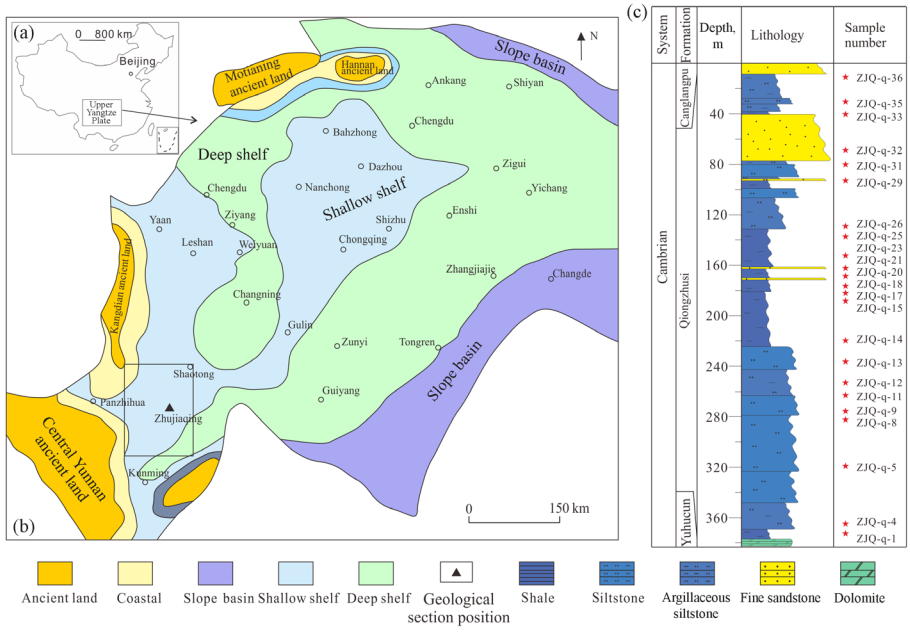

Fig. 1. a) and b) Location and geological map of the study area; c) a profile histogram of the study area.

two members. The lower Hongjingshao Member is gray or gray-green fine sandstone intercalated with shale, siltstone and purple-red mud shale. The upper Wulongqing Member is gray-yellow or gray-green siltstone, the shale is sandwiched between homochromatic sandstone and argillaceous dolomite. The lower part of the succession is composed mostly of gravel-bearing sandstone or conglomerate.

3. Methods and material

A total of twenty-three fresh outcrop shale samples from the QZS Formation were initially polished to remove the weathered surfaces (Fig. 2a–d). The organic-free samples were analyzed for their major and trace element concentrations in the State Key Laboratory of Continental Dynamics, Northwest University in Xi'an, China. The total organic carbon (TOC) was determined for 23 samples, using a CS-580A instrument following the standard of HJ 695-2014, at Beijing Research Institute of Uranium Geology, China National Nuclear Corporation.

The samples were removed and powdered using a tungsten carbide ball mill to pass through a 200-mesh sieve. Major elements were analyzed by an X-ray fluorescence (XRF) Rigaku RIX 2100 spectrometer using the United States Geological Survey (USGS) and Chinese national rock standards BCR-2,

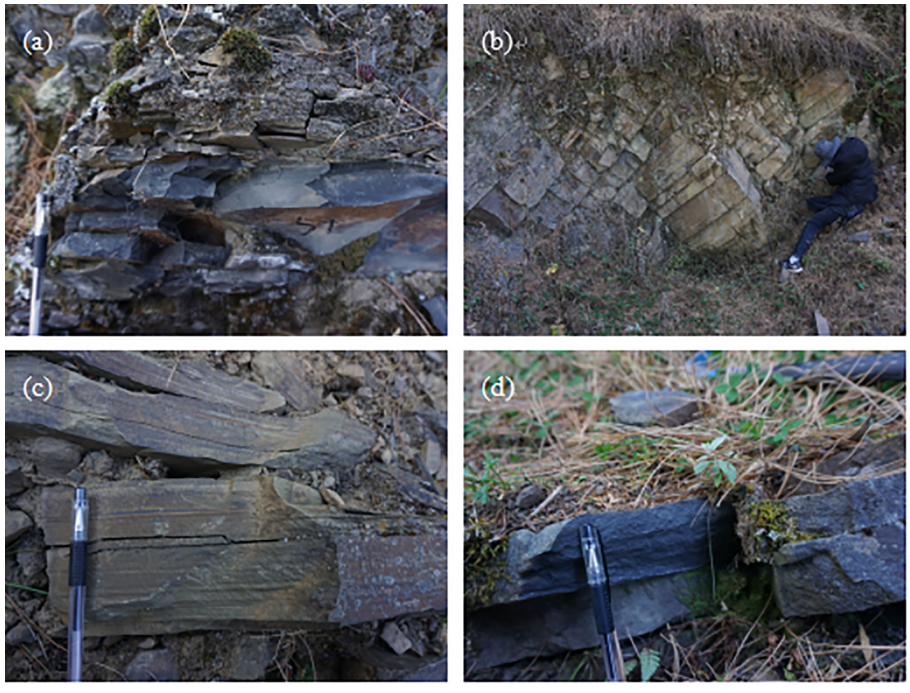

Fig. 2. Representative outcrop photographs of the studied black shale.

GSR-1 and GSR-3 for calibration. The accuracy and precision of experimental analysis for the major elements were generally better than 5%. For the trace element analysis, sample powders were digested using an HF + HNO_3 mixture in high-pressure Teflon bombs at 190 °C for 48 h. For the trace elements, the analytical error was less than 2% and the precision was better than 10% [24].

4. Results

4.1. Major elements and TOC content

The results of the chemical analysis of the major oxides of the QZS Formation shale are presented in Table 1. The main components of the Formation's sample are SiO_2, Al_2O_3 and total Fe_2O_3 (TFe_2O_3). Among them, the SiO_2 content is the highest, ranging from 51.44 to 78.23 wt%, with an average value of 64.08 wt%. The TFe_2O_3 content ranges from 2.16 to 7.83 wt%, with an average value of 5.39 wt%. The Al_2O_3 content varies between 7.62 and 20.54 wt% in all samples. The amount of CaO in the study area is 0.03–7.27 wt%, with an average value of 1.06 wt%. The content of MnO ranges from 0.01 to 0.28 wt%, with an average value of 0.06 wt%. The total organic carbon (TOC) content ranges from 0.07 to 2.09%, averaging 0.39%. Although the TOC of the Qiongzhusi Formation outcrop in the study area is not high, the Cambrian Qiongzhusi Formation reservoir in the Sichuan Basin, which is adjacent to its northern part, has a wide distribution range, a large thickness, a high gas content and a large total resource amount. The hydrocarbon source rock of the Lower Cambrian Qiongzhusi Formation is the main hydrocarbon source rock of the Sinian-Ordovician gas system, which has been widely recognized [25, 26].

4.2. Trace elements

Trace element concentrations of QZS shale samples are listed in Table 2. In order to analyze the enrichment of elements, we carried out the upper continental crust standardization for trace elements [27]. Figure 3 shows that most redox-sensitive elements, such as V, Cr, Ni, Zn and U, are enriched compared to UCC. Except for V, Cu and Pb, whose content fluctuates greatly, that of other elements is relatively consistent. The concentration of large-ionic-radius lithophile elements, such as Ba (320–979 ppm) and Rb (47.9–175 ppm), and high-field-strength elements, such as Th (6.09–16.9 ppm) and Ta (0.54–1.22 ppm), are similar to the respective UCC values. Some trace elements, such as Co (17.9–191 ppm), Ni (20.9–83.7 ppm) and U (1.78–18.3 ppm), are enriched with respect to UCC. The Sr element content (10.4–95.4 ppm) is lower than that in UCC.

Table 1. Major compound concentrations and TOC content in the Qiongzhusi shale, wt%

Sample No.	SiO_2	TiO_2	Al_2O_3	TFe_2O_3	MnO	MgO	CaO
ZJQ-q-36	54.58	0.59	13.13	4.78	0.09	6.21	5.46
ZJQ-q-35	70.37	0.60	12.40	6.12	0.06	2.84	0.20
ZJQ-q-33	51.44	0.66	15.80	5.01	0.08	5.52	5.24
ZJQ-q-32	60.57	0.35	8.70	4.12	0.14	4.56	7.27
ZJQ-q-31	78.23	0.50	7.62	5.46	0.17	2.38	0.09
ZJQ-q-29	57.15	0.77	20.54	6.18	0.05	3.59	0.10
ZJQ-q-26	58.03	0.78	19.26	7.67	0.09	3.45	0.06
ZJQ-q-25	56.75	0.77	20.04	7.64	0.04	3.55	0.03
ZJQ-q-23	68.54	0.65	12.91	6.92	0.28	2.69	0.08
ZJQ-q-21	56.79	0.81	19.84	7.82	0.05	3.65	0.10
ZJQ-q-20	57.19	0.77	19.66	7.83	0.08	3.58	0.06
ZJQ-q-18	70.17	0.57	12.38	6.63	0.17	2.16	0.08
ZJQ-q-17	57.15	0.75	19.77	7.28	0.04	3.35	0.08
ZJQ-q-15	63.55	0.85	16.89	4.22	0.01	2.12	0.04
ZJQ-q-14	67.64	0.99	15.71	2.16	0.01	1.24	0.10
ZJQ-q-13	71.29	0.83	13.69	3.23	0.01	0.76	0.14
ZJQ-q-12	68.79	0.72	13.80	4.84	0.04	1.07	0.43
ZJQ-q-11	67.15	0.67	14.84	4.42	0.02	2.38	0.44
ZJQ-q-9	67.24	0.70	12.81	3.62	0.03	1.89	2.57
ZJQ-q-8	69.36	0.68	13.46	4.21	0.04	2.02	0.51
ZJQ-q-5	67.08	0.78	13.79	5.39	0.06	2.55	0.47
ZJQ-q-4	68.53	0.73	13.65	4.02	0.01	1.90	0.55
ZJQ-q-1	66.20	0.75	13.58	4.33	0.01	1.17	0.24

Table 1. (continued)

Na_2O	K_2O	P_2O_5	LOI	TOTAL	[1]CIA	[2]CIW	[3]PIA	TOC
0.07	3.69	0.17	11.20	99.97	75.66	98.28	52.64	0.101
0.09	3.23	0.17	3.66	99.74	77.50	99.16	55.65	0.072
0.09	4.72	0.21	10.98	99.75	74.51	98.16	50.42	0.105
0.06	2.52	0.15	11.17	99.61	74.84	97.78	51.38	0.098
0.05	1.65	0.17	3.25	99.57	82.42	102.16	63.11	0.069
0.07	5.60	0.16	5.39	99.60	77.47	100.42	54.61	0.154
0.20	4.37	0.21	5.62	99.74	80.50	100.34	60.73	0.107
0.07	4.63	0.15	5.87	99.54	80.61	100.95	60.45	0.164
0.62	2.33	0.08	4.69	99.79	78.69	92.99	63.32	0.174
0.30	4.52	0.19	5.65	99.72	79.51	98.90	59.90	0.236
0.22	4.31	0.17	5.97	99.84	80.61	99.68	61.48	0.111
1.07	2.28	0.12	3.98	99.61	75.18	88.44	60.20	0.618
0.10	4.45	0.17	6.58	99.72	80.73	100.49	61.06	2.09
0.09	4.33	0.13	7.54	99.77	78.61	100.54	56.80	1.31
1.90	4.96	0.33	4.56	99.59	66.58	86.19	43.83	0.295
2.61	4.04	0.21	2.97	99.77	61.92	77.19	42.14	0.205
1.85	4.22	0.31	3.46	99.53	64.33	81.74	43.04	0.126
2.33	4.10	0.25	3.11	99.71	63.66	78.63	44.62	0.135
2.39	3.73	0.31	4.43	99.72	51.84	61.97	35.50	0.29
2.44	3.71	0.30	3.03	99.76	62.03	76.12	43.53	0.15
2.41	3.50	0.30	3.32	99.65	63.61	77.08	46.14	0.154
2.26	4.21	0.27	3.38	99.51	61.27	77.03	40.82	0.149
1.60	4.90	0.33	6.45	99.56	64.17	85.63	39.11	2.08

LOI – loss on ignition; [1]CIA – chemical index of alteration; [2]CIW – chemical index of weathering; [3]PIA – plagioclase index of alteration

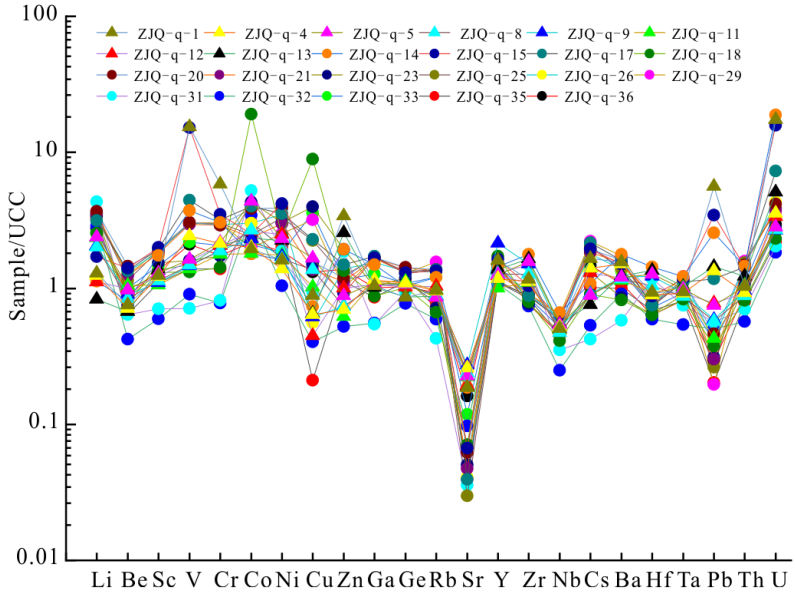

Fig. 3. UCC-normalized trace elements spider diagrams of samples from the Qiongzhusi Formation in the Zhujiaqing section.

4.3. Rare earth elements

Rare earth element concentrations of QZS shale are presented in Table 2. The total concentration of REE (∑REE) of QZS shale is 174.58 ppm on average, which is slightly higher than that of UCC (average 146.37 ppm) [27] and the North American Shale Composite (NASC) (average 173.21 ppm) [28]. The total concentration of light rare earth elements (ΣLREE) of QZS shale is 76.63–258.99 ppm (average value 155.16 ppm) and makes up 89% of ΣREE, which is higher than the average value of Chinese and Australian oil shales, 61.48 ppm and 63.00 ppm, respectively [29, 30]. The total concentration of heavy rare earth elements (ΣHREE) of QZS shale is 5.28–9.36 ppm (average value 7.45 ppm) and makes up only 4% of ΣREE, which is also higher than the average value of Chinese oil shales (6.71 ppm [29]), but lower than that of Australian oil shales (average value 14.40 ppm [30]). The concentration of middle rare earth elements (MREE) of QZS shale is between 8.77 and 17.58 ppm, averaging 11.97 ppm.

REE abundances of QZS shale are normalized to chondrites (Fig. 4a). The chondrite-normalized REE diagram shows LREE to be enriched. The steeper LREE partition curve in the La-Eu section indicates that the degree of fractionation among LREE is rather high. However, the diagram is characterized by a relatively flat pattern in the Gd-Lu section. The NASC-normalized patterns (Fig. 4b) show rather flat paters with larger variation in LREE relative to it.

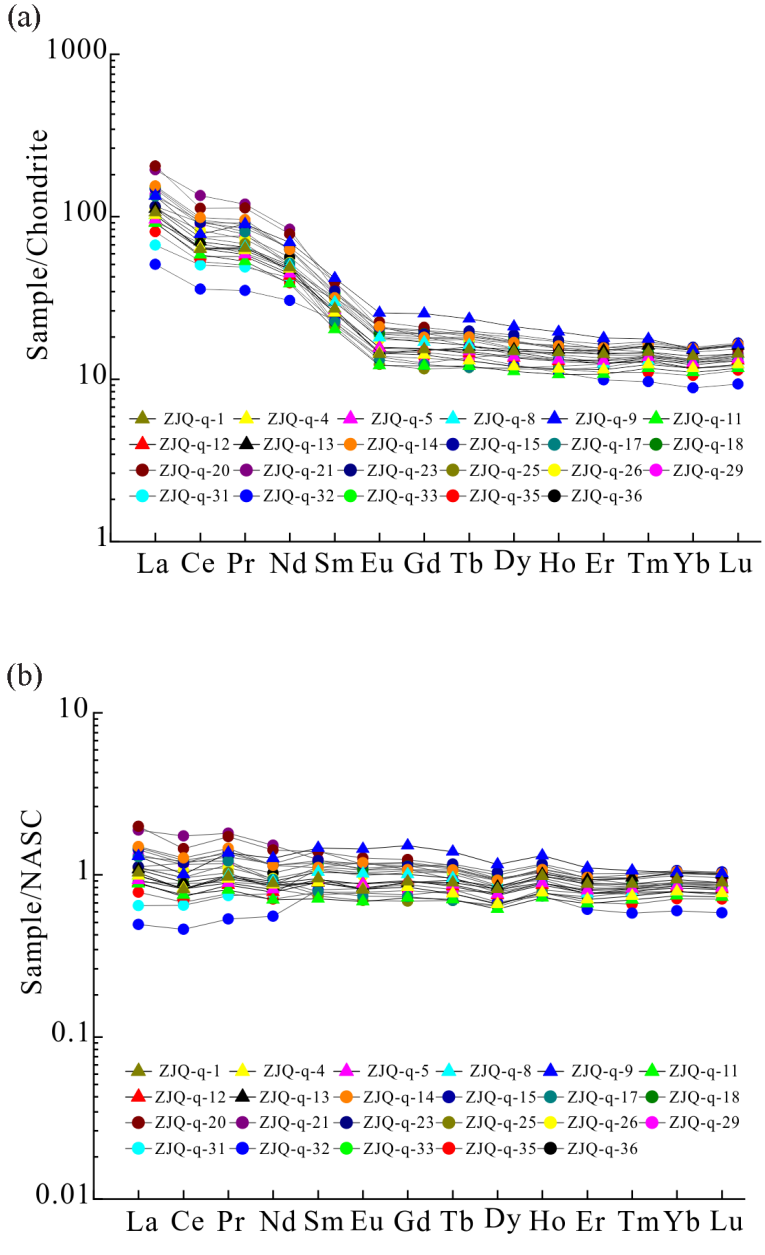

Fig. 4. a) Chondrite-normalized REE distribution patterns of samples from the Qiongzhusi Formation in the Zhujiaqing section; b) NASC-normalized REE distribution patterns of samples from the QZS Formation in the Zhujiaqing section.

Table 2. Trace and rare earth element concentrations in Qiongzhuzi shale samples, ppm

Sample No.	Li	Be	Sc	V	Cr	Co	Ni	Cu	Zn	Ga	Ge	Rb	Sr	Y	Zr	Nb	Cs
ZJQ-q-36	54.9	2.64	14.9	126	61.2	21.7	37.4	33	98.2	17.2	1.65	104	56.4	33.1	145	11.4	5.46
ZJQ-q-35	65.2	1.94	12.1	83.5	48.5	30.5	40.2	5.26	80.2	14.6	1.79	88.6	23.7	24.4	160	11.3	3.75
ZJQ-q-33	51.6	3.01	16.2	131	72.3	20.9	36.8	89.8	82.2	21.7	1.74	136	41.4	29.8	162	12.9	7.66
ZJQ-q-32	57.6	1.27	6.58	54.2	27.2	34.5	20.9	10.1	37.2	9.44	1.24	66.2	34	23.7	140	6.25	1.97
ZJQ-q-31	86.6	1.92	7.79	42.7	28.6	52.2	37.8	23.5	132	9.23	1.51	47.9	12.5	28.5	284	8.8	1.56
ZJQ-q-29	66.3	3.72	21.3	182	106	19.9	50.6	79.8	71.7	28.4	2.07	175	13.9	29.6	174	16	8.21
ZJQ-q-26	66.7	3.95	20.5	181	103	30	69.9	14	98.3	26.3	2.13	148	14.3	32.2	173	15.1	6.62
ZJQ-q-25	70.2	3.43	20.9	181	105	24.8	65.9	56.3	87.5	28.3	2.14	154	10.4	25	165	14.9	7.39
ZJQ-q-23	68.5	2.25	17	96.1	60.6	43.1	60.9	99.2	137	17.5	1.91	80.3	17.7	31.9	146	12	4.88
ZJQ-q-21	71.3	3.72	19.8	177	102	23.5	59.9	34.3	79.5	28.2	2.26	152	16.6	27.5	174	15.8	6.81
ZJQ-q-20	73.6	4.37	20.9	183	102	38.5	78.2	39	84.8	28.7	2.28	154	21.7	32.1	170	15	7.18
ZJQ-q-18	50.9	2.55	14.4	78.9	50	191	48.6	223	95.6	14.9	1.63	74.5	24.8	37.8	151	10.3	3.34
ZJQ-q-17	62.9	4.03	21.5	267	112	40.1	70.8	57.2	106	29.3	2.06	154	13.8	24.3	167	14.6	8
ZJQ-q-15	34.3	4.23	22	913	122	25.1	83.7	37.4	65.6	28.5	2.08	151	23.4	36	198	15.2	7.22
ZJQ-q-14	22.6	2.43	19.2	224	107	17.9	32.4	18.4	137	25.4	1.66	135	65.1	31.7	337	16.5	4.01
ZJQ-q-13	16.6	2.03	15	89.6	72.8	23.3	44.9	16.3	182	17.3	1.38	97.9	66.2	30.4	312	13.7	2.8
ZJQ-q-12	22.2	3	13.4	95.4	72.4	26.3	49.7	11.2	71.4	18.2	1.64	116	67.8	27.1	209	12.4	4.82
ZJQ-q-11	46.9	3.14	11.6	83.1	62.1	18	35.1	25.6	44	19.1	1.79	109	78	22.1	210	12.5	5.24
ZJQ-q-9	41	2.7	12.1	87.5	66.8	23.1	34.2	15.4	52.4	17.9	1.72	99.4	95.4	47.2	287	12.7	3.37
ZJQ-q-8	40.1	2.51	12.5	88.8	66.1	26.8	32.9	34.3	52	18	1.71	99.1	83.5	28.1	241	11.8	3.32
ZJQ-q-5	47.7	2.91	14.2	98.2	76.2	43.7	46.4	41.6	62.4	18.7	1.72	96	79.5	27.8	299	13.5	3.28
ZJQ-q-4	24.8	2.13	13.4	146	74.6	20	27.8	16	49.5	19.5	1.75	107	90.9	25.9	213	12.9	5.22
ZJQ-q-1	25.9	2.26	13.7	920	204	19.5	32.3	22.2	241	17.7	1.37	108	65.2	35.2	221	12.7	6.11

Table 2. (continued)

Ba	Hf	Ta	Pb	Th	U	La	Ce	Pr	Nd	Sm	Eu	Gd	Tb	Dy	Ho	Er	Tm	Yb	Lu
598	3.68	0.82	5.86	9.59	2.87	35.3	70.3	9.15	33.8	6.76	1.46	6.2	0.94	5.4	1.08	2.96	0.42	2.72	0.42
549	4	0.81	4.05	8.47	2.12	25	49.6	6.05	23.4	4.46	0.97	4.16	0.65	3.85	0.81	2.31	0.33	2.21	0.34
738	4.19	0.93	8.16	11.6	3.59	47	89.6	10.7	37.9	6.78	1.36	5.94	0.86	4.9	0.99	2.83	0.41	2.75	0.42
501	3.44	0.54	10.1	6.09	1.78	15.8	33.7	4.22	18.3	4.61	1.02	4.53	0.69	3.93	0.77	2.08	0.29	1.86	0.28
320	6.84	0.75	11.3	7.53	1.97	20.7	47.4	5.87	25.3	6.24	1.28	5.51	0.89	4.99	0.97	2.65	0.38	2.45	0.36
951	4.56	1.22	3.93	16.9	3.56	42.8	84.6	9.31	30	4.3	0.96	3.9	0.68	4.55	1.02	3.09	0.48	3.23	0.49
761	4.52	1.14	8.38	15.6	4.18	34.4	77.5	8.75	31.3	6.12	1.23	5.36	0.88	5.34	1.13	3.27	0.48	3.2	0.48
769	4.28	1.12	5.25	16.5	3.71	35.7	69.9	8.16	27	4.21	0.86	3.58	0.59	3.76	0.84	2.6	0.41	2.78	0.43
469	3.74	0.9	6.23	11.4	2.64	35.9	86.4	10.2	38.7	7.98	1.44	6.12	0.92	5.47	1.1	3.05	0.43	2.68	0.39
847	4.39	1.16	6.04	15.9	3.72	60.4	127	14.3	50.2	7.09	1.33	5.64	0.8	4.54	0.92	2.76	0.42	2.8	0.43
889	4.39	1.15	9.26	15.9	4.04	63.6	106	13.6	46.9	7.9	1.58	6.47	0.97	5.51	1.09	3.18	0.47	3.08	0.46
452	3.69	0.83	7.5	8.72	2.25	28.9	64.4	7.13	28.6	6.39	1.33	5.88	0.96	5.79	1.19	3.22	0.44	2.75	0.41
882	4.34	1.11	23.4	15.3	7.05	41.3	88.9	9.63	30.9	4.49	0.92	3.81	0.59	3.7	0.8	2.49	0.39	2.66	0.41
823	5.07	1.18	68.9	15.3	15.3	45.8	86.1	11	37.7	6.96	1.45	5.85	0.99	6	1.21	3.45	0.51	3.3	0.5
979	8.3	1.22	51.1	15.5	18.3	47.9	92.9	11.5	37.7	6.34	1.47	5.6	0.91	5.38	1.12	3.27	0.5	3.24	0.49
679	7.83	1.03	28.8	13.1	4.95	34.5	65.8	7.77	28.1	5.08	1.03	4.63	0.79	4.89	1.05	3.16	0.48	3.16	0.48
655	5.16	0.92	15.6	9.87	3.27	28.6	53.6	6.82	25.8	5.13	1.1	4.8	0.72	4.33	0.9	2.62	0.4	2.57	0.39
628	5.41	1.01	8.58	11.2	2.6	28.3	54.8	6.38	23.2	4.05	0.85	3.75	0.6	3.57	0.75	2.26	0.35	2.31	0.35
666	7.11	0.93	11.8	10.3	2.6	41.7	73.5	10.8	41.7	8.36	1.79	7.87	1.18	6.74	1.37	3.76	0.53	3.21	0.49
647	6.05	0.87	11.5	9.43	2.61	31.6	59.8	7.83	30.1	5.95	1.26	5.23	0.81	4.7	0.93	2.61	0.39	2.45	0.37
661	7.37	0.99	15	11	2.74	29.7	59.9	7.03	26.8	5.32	1.09	4.72	0.74	4.39	0.92	2.72	0.41	2.65	0.4
833	5.18	0.92	26.9	9.95	3.46	31.6	60.6	7.46	28.7	5.11	1.01	4.38	0.65	3.82	0.81	2.4	0.37	2.45	0.37
859	5.43	0.94	112	11	16.9	33	59.2	7.68	29.2	5.42	1	4.73	0.76	4.74	1.02	2.99	0.44	2.9	0.43

5. Discussion

5.1. Provenance

It has been demonstrated that the chemical composition of siliciclastic sedimentary rocks is related to that of their source regions and can be used to characterize the source rocks from which the investigated siliciclastic sedimentary rocks were derived [31–34]. Bhatia and Crook [35] found that siliciclastic rocks deposited in various tectonic environments differ markedly in major element compositions. This holds true also for limestones [36]. The ratio of $w(SiO_2)/w(Al_2O_3)$ in the analyzed samples ranges from 2.78 to 10.26, with an average of 4.63, which is slightly higher than that of the continental crust average (3.6) [27]. This indicates that the sediments were primarily derived from continental clastic material [37–39]. The $w(SiO_2)/w(Al_2O_3)$ ratios of most clastic rocks are chiefly used to infer the source rock compositions [40]. The $w(Al_2O_3)/w(TiO_2)$ ratio increases from 3 to 8 for mafic igneous rocks, from 8 to 21 for intermediate rocks, and from 21 to 70 for felsic igneous rocks [40]. The $w(Al_2O_3)/w(TiO_2)$ ratio of QZS shale ranges from 15.24 to 26.68, averaging 21.24, which suggests that felsic intermediate igneous rocks were probably the source rocks for the QZS Formation shale.

$Zr\text{-}TiO_2$ diagram can be used to discriminate the provenance of sedimentary rocks [40]. The $Zr\text{-}TiO_2$ diagram of QZS shale shows that the source region of detritus originates from the erosion of felsic igneous rocks (Fig. 5a). The Th/Sc vs Zr/Sc plot (Fig. 5b) was used to infer the provenance of the QZS black shale [41]. The samples in the felsic field suggest that felsic rock may be the dominating source of the sediments.

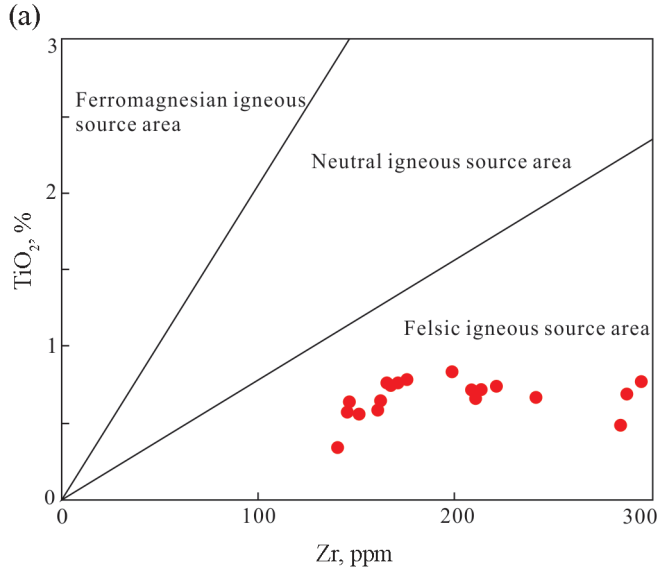

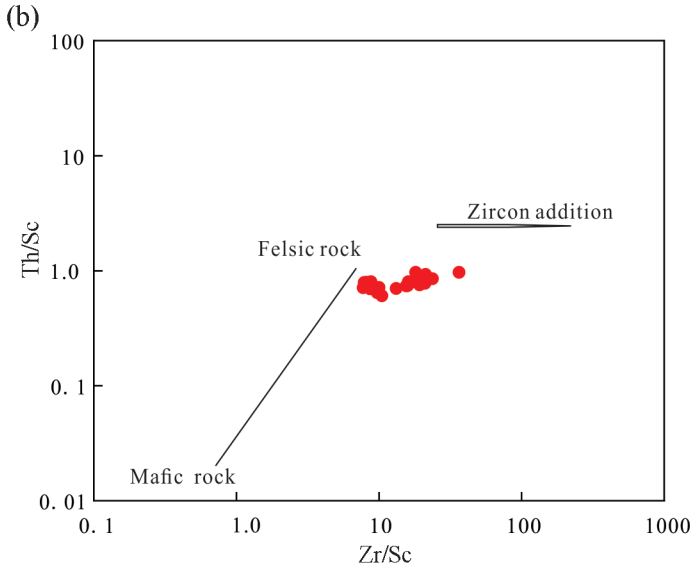

Fig. 5. Provenance discrimination diagrams: a) TiO2 vs Zr [40]; b) Th/Sc vs Zr/Sc [41].

Also, the discriminant function of F1 vs F2 and F3 vs F4 by Roser and Korsch [42] has been plotted in order to determine the provenance of QZS shale. The QZS samples mostly plot in the quartzite sediment provenance zone, except for three samples that plot in the felsic igneous provenance (Fig. 6a–b). The results show that there was a relatively stable material source during the depositional period of the QZS Formation and that the mineral maturity of the parent rock was moderate.

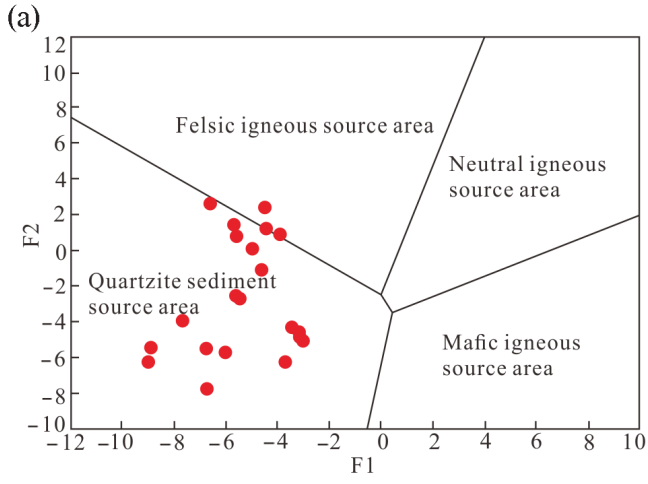

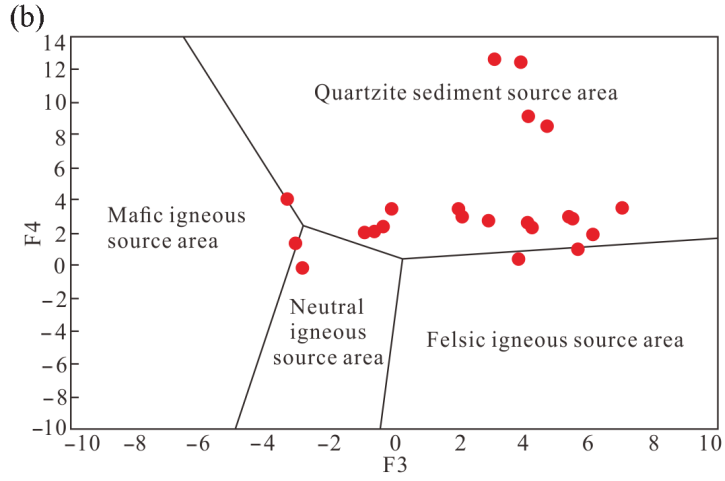

Fig. 6. Source region discrimination based on principal element analysis [42].

In addition, the provenance was analyzed based on the discrimination diagram of ∑REE vs La/Yb [43] (Fig. 7). Data show that QZS Formation samples chiefly fall within the region of sedimentary rocks and the intersectional region of granite and sedimentary rocks.

In general, the provenance analysis suggests sedimentary and felsic igneous rocks to be the dominant provenance of QZS shale. This is consistent with the provenance of rock types present in the uplifted Kangdian Ancient Land to the west of the Upper Yangtze Plate in the Early Cambrian, which include granites and sedimentary rocks enriched with felsic minerals [8, 44–46].

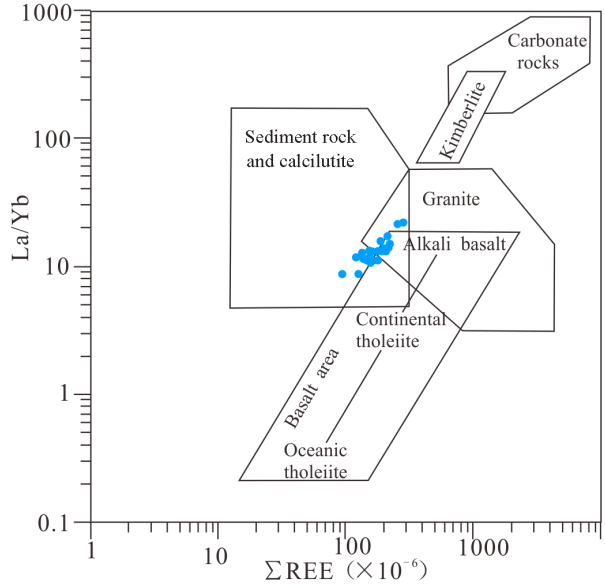

Fig. 7. Discrimination diagrams for the provenance attributes of the shale in the Qiongzhusi Formation (base map source [43]).

5.2. Paleoweathering

The chemical weathering of source rocks can be assessed using the chemical index of alteration proposed by Nesbitt and Young [16], the chemical index of weathering which removes K_2O to eliminate the influence of potassium metasomatism [47], and the plagioclase index of alteration which adjusts the K_2O and Al_2O_3 contribution from potassium feldspar and monitors the degree of plagioclase weathering that has been successfully used for the reconstruction of paleoweathering [48–58].

These proxies are defined using the following formulas:

$$CIA = 100 \times Al_2O_3/(Al_2O_3 + CaO^* + Na_2O + K_2O), \quad (1)$$

$$CIW = 100 \times Al_2O_3/(Al_2O_3 + CaO^* + Na_2O), \quad (2)$$

$$PIA = 100 \times (Al_2O_3 - K_2O)/(Al_2O_3 + CaO^* + Na_2O + K_2O). \quad (3)$$

CaO* represents the fraction of CaO in silicate minerals, which is used in place of total CaO to avoid the contribution of CaO from carbonate and phosphate minerals that are not linked to weathering processes [16]. CaO* is derived using the following formula (in moles): $CaO^* = CaO - (10/3) \times P_2O_5$. If CaO* was less than the moles of Na_2O, this CaO value was adopted. Otherwise, CaO* was assumed to be equivalent to Na_2O [17, 59].

The calculated chemical weathering indices, including CIA, CIW and PIA, are given in Table 1. The CIA value of QZS shale ranges from 51.8 to 82.4, with an average value of 72. The shale's CIW value is in the range from 61.97 to 102.2, averaging 90.43, while its PIA value is between 35.5 and 63.3, with an average of 51.8. McLennan et al. [41] demonstrated that the CIA value of 50–65 indicates limited weathering, the value between 65 and 85 refers to moderate weathering, and the value from 85 to 100 suggests strong chemical weathering in a hot and humid climate.

The CIA, CIW and PIA of the Qiongzhusi Formation of the Zhujiaqing section are given in Figure 8. A good correlation among the CIA, PIA and CIW values can be observed. The studied succession can be subdivided into two stages: Stage 1 (Lower Qiongzhusi Formation) and Stage 2 (Upper Qiongzhusi Formation) (Fig. 8). In Stage 1, the CIA ranges from 51.84 to 64.33, with an average value of 61.61, indicating limited weathering in a cold and dry climate. In Stage 2, the CIA values are somewhat higher, ranging from 66.58 to 82.42, with an average of 77.56, indicating moderate chemical weathering, probably in humid climates. This evidences that Stage 2 was deposited in a warmer and more humid climate than Stage 1 under stronger weathering conditions.

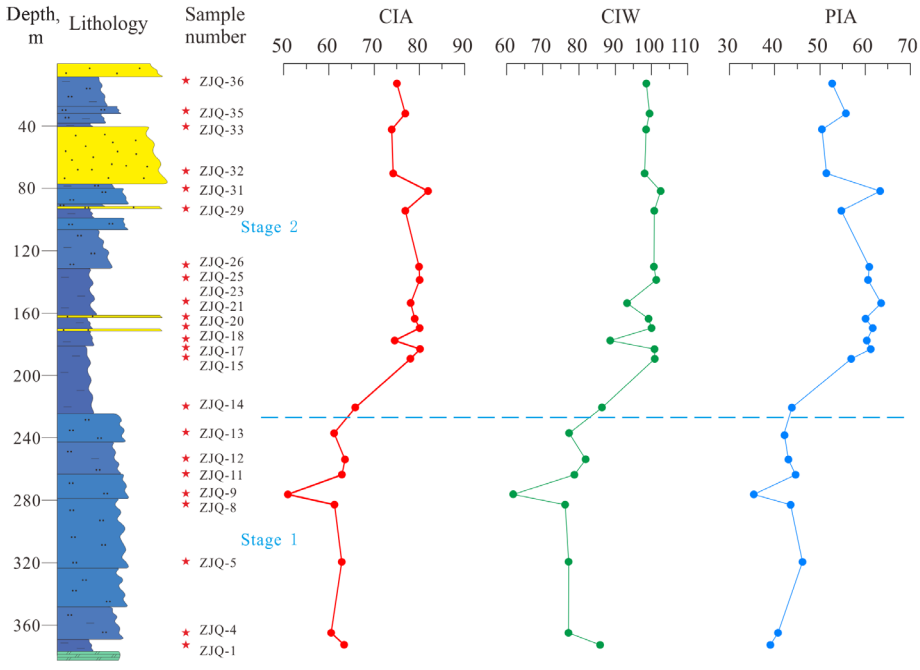

Fig. 8. Chemical weathering indices and element ratios of the Qiongzhusi Formation of the Zhujiaqing section.

The changing trend of CIW and PIA values for the QZS Formation sediments follows a similar pattern to that of CIA values, which further supports lower weathering intensity during Stage 1 compared to Stage 2. The CIW values ranged from 86.19 to 102.16, with a mean of 97.63 in Stage 2, thus displaying an intense degree of weathering of the source material. This is a strong indication that secondary K enrichment has overprinted the CIA values of the primary mineral matter in Stage 2. Nevertheless, the source and timing of the possible secondary K enrichment remain elusive. Previously it has been suggested that hydrothermal action was involved in the deposition of sedimentary rocks of the QZS Formation, which may have contributed to the enrichment of potassium in the considered black shales [22]. However, it should be pointed out that in reality, tuffaceous rocks, granites and upper crustal felsic rocks such as sedimentary rocks rich in felsic minerals are developed in the Kangdian Ancient Land in the western part of the study area. The physical and chemical erosional products of these felsic minerals-rich sedimentary rocks may have well contributed to potassium enrichment in the studied black shales.

The A-CN-K ternary diagram (Fig. 9) can be used to evaluate the mobility of elements and recognize the post-depositional diagenetic and metasomatic influences on clastic sediments [17]. The results show a linear trend

subparallel to the A-CN connection line in the A-CN-K triangle, suggesting the sustained weathering of primarily granite rocks. This result is consistent with the previous expression that granite is one of the sources of QZS shales. The partial distribution of samples in Stage 2 is indicative of their inclination towards the K_2O apex, implying that these samples underwent potassium metasomatism during diagenesis.

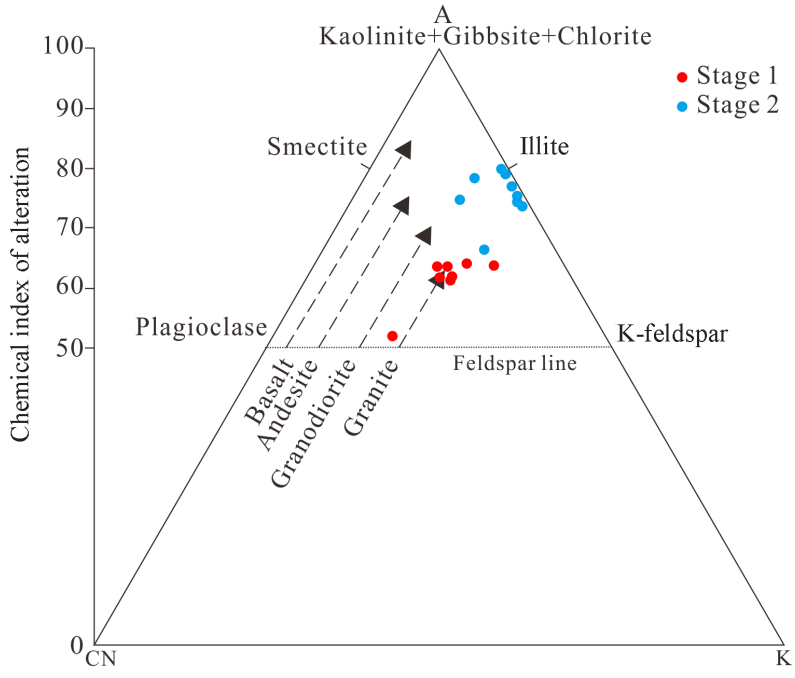

Fig. 9. Ternary diagrams of A-CN-K for the Qiongzhusi Formation samples from the Zhujaiqing section based on the method described by Fedo et al. [17]. Abbreviations: A – Al_2O_3, CN – CaO* + Na_2O, K – K_2O.

6. Conclusions

The main components of the Qiongzhusi shale are SiO_2, Al_2O_3 and TFe_2O_3, with the average values of 64.08%, 15.00% and 5.39%, respectively. The shale's redox-sensitive elements, such as V, Cr, Ni, Zn and U, are richer compared to the upper continental crust. The total concentration of rare earth elements of QZS shale is 174.58 ppm, which is higher than that of UCC (average 146.37 ppm) and the North American Shale Composite (average 173.21 ppm).

The ratios of $w(SiO_2)/w(Al_2O_3)$, $w(Al_2O_3)/w(TiO_2)$, the Zr-TiO_2 diagram, the Th/Sc vs Zr/Sc plot, the discriminant function of F1 vs F2 and F3 vs F4,

and the discrimination diagram of the total concentration of REE vs La/Yb indicated that sedimentary and felsic igneous rocks are the main provenances of QZS shale. The values of chemical weathering indices – the chemical index of alteration, the chemical index of weathering and the plagioclase index of alteration, – of the Lower QZS Formation (Stage 1) are lower than those of the Upper QZS Formation (Stage 2). This chemical weathering index indicates that Stage 2 was deposited in a warmer and more humid climate than Stage 1 under stronger weathering conditions.

Acknowledgments

This research was supported by the National Natural Science Foundation of China (Nos. 42130206, 41302076). Thanks are due to both reviewers for their abundant critical and constructive comments.

The publication costs of this article were partially covered by the Estonian Academy of Sciences.

REFERENCES

1. Cloud, Jr, P. E. Some problems and patterns of evolution exemplified by fossil invertebrates. *Evolution*, 1948, **2**(4), 322–350.
2. Butterfield, N. J. Macroevolutionary turnover through the Ediacaran transition: ecological and biogeochemical implications. *Geol. Soc., London, Spec. Publ.*, 2009, **326**(1), 55–66.
3. Shu, D., Isozaki, Y., Zhang, X., Han, J., Maruyama, S. Birth and early evolution of metazoans. *Gondwana Res.*, 2014, **25**(3), 884–895.
4. Cawood, P. A., Wang, Y., Xu, Y., Zhao, G. Locating South China in Rodinia and Gondwana: A fragment of greater India lithosphere? *Geology*, 2013, **41**(8), 903–906.
5. Jin, C., Li, C., Algeo, T. J., Wu, S., Cheng, M., Zhang, Z., Shi, W. Controls on organic matter accumulation on the early-Cambrian western Yangtze Platform, South China. *Mar. Petrol. Geol.*, 2020, **111**, 75–87.
6. Maloof, A. C., Ramezani, J., Bowring, S. A., Fike, D. A., Porter, S. M., Mazouad, M. Constraints on early Cambrian carbon cycling from the duration of the Nemakit-Daldynian–Tommotian boundary δ13C shift, Morocco. *Geology*, 2010, **38**(7), 623–626.
7. Cremonese, L., Shields-Zhou, G., Struck, U., Ling, H.-F., Och, L., Chen, X., Li, D. Marine biogeochemical cycling during the early Cambrian constrained by a nitrogen and organic carbon isotope study of the Xiaotan section, South China. *Precambrian Res.*, 2013, **225**, 148–165.
8. Jin, C., Li, C., Algeo, T. J., Planavsky, N. J., Cui, H., Yang, X., Zhao, Y., Zhang, X., Xie, S. A highly redox-heterogeneous ocean in South China during

the early Cambrian (~ 529–514 Ma): Implications for biota-environment co-evolution. *Earth Planet. Sci. Lett.*, 2016, **441**, 38–51.

9. Xiao, X. M., Wei, Q., Gai, H. F., Li, T. F., Wang, M. L., Pan, L., Chen, J., Tian, H. Main controlling factors and enrichment area evaluation of shale gas of the Lower Paleozoic marine strata in south China. *Petrol. Sci.*, 2015, **12**(4), 573–586.
10. Zhu, M. Y., Sun, Z. X., Yang, A. H., Yuan, J. L., Li, G. X., Zhou, Z. Q., Zhang, J. M. Lithostratigraphic subdivision and correlation of the Cambrian in China. *Journal of Stratigraphy*, 2021, **45**(3), 223–249 (in Chinese).
11. Ketris, M. P., Yudovich, Ya. E. Estimations of clarkes for carbonaceous biolithes: world average for trace element contents in black shales and coals. *Int. J. Coal Geol.*, 2009, **78**(2), 135–148.
12. Song, Y., Li, S., Hu, S. Warm-humid paleoclimate control of salinized lacustrine organic-rich shale deposition in the Oligocene Hetaoyuan Formation of the Biyang Depression, East China. *Int. J. Coal Geol.*, 2019, **202**, 69–84.
13. Algeo, T. J., Liu, J. S. A re-assessment of elemental proxies for paleoredox analysis. *Chem. Geol.*, 2020, **540**, 119549.
14. Li, D., Chen, Y., Wang, Z., Lin, Y., Zhou, J. Paleozoic sedimentary record of the Xing-Meng Orogenic Belt, Inner Mongolia: Implications for the provenances and tectonic evolution of the Central Asian Orogenic Belt. *Chinese Sci. Bull.*, 2012, **57**(7), 776–785.
15. Mondal, M. E. A., Wani, H., Mondal, B. Geochemical signature of provenance, tectonics and chemical weathering in the Quaternary flood plain sediments of the Hindon River, Gangetic plain, India. *Tectonophysics*, 2012, **566−567**, 87−94.
16. Nesbitt, H. W., Young, G. M. Early Proterozoic climates and plate motions inferred from major element chemistry of lutites. *Nature*, 1982, **299**(5885), 715–717.
17. Fedo, C. M., Nesbitt, H. W., Young, G. M. Unraveling the effects of potassium metasomatism in sedimentary rocks and paleosols, with implications for paleoweathering conditions and provenance. *Geology*, 1995, **23**(10), 921–924.
18. Raza, M., Ahmad, A. H. M., Shamim Khan, M., Khan, F. Geochemistry and detrital modes of Proterozoic sedimentary rocks, Bayana Basin, north Delhi fold belt: implications for provenance and source-area weathering. *Int. Geol. Rev.*, 2012, **54**(1), 111–129.
19. Zhang, D. Y. *Geochemical Characteristics of the Heiyi Rock Series in the Lower Cambrian Qiongzhusi Formation in the Huize Area of Northeastern Yunnan*. Master's Thesis. KunMing University of Science and Technology, China, 2017 (in Chinese).
20. Cheng, Y., Hu, Y. Z., Li, P. Y., Lu, P. The geochemical characteristics of trace elements and paleoenvironmental evolution of black rock series in the lower Cambrian Qiongzhusi Formation from Huize area, eastern Yunnan province. *Contributions to Geology and Mineral Resources Research*, 2019, **34**(3), 416–422 (in Chinese).

21. Fang, Z. X. *Sedimentary Environment and Source Rock Characteristics of Black Shale in the Lower Cambrian Qiongzhusi Formation, Eastern Yunnan*. Master's Thesis. Northwest University, China, 2020 (in Chinese).
22. Cheng, Y., Jian, L., Tang, G., Zhang, C. Trace Element Anomaly Characteristics and Metallogenic Significance of the Lower Cambrian Qiongzhusi Formation from Huize Area, Eastern Yunnan Province. *Nonferrous Metals Engineering*, 2020, **10**(12), 90–98 (in Chinese).
23. Li, J. H., Wang, H. H., Li, W. B., Zhou, X. B. Discussion on global tectonics evolution from plate reconstruction in Phanerozoic. *Acta Petrolei Sinica*, 2014, **35**(2), 207–218 (in Chinese).
24. Liu, Y., Liu, X. M., Hu, Z. C., Diwu, C. R., Yuan, H. L., Gao, S. Evaluation of accuracy and long-term stability of determination of 37 trace elements in geological samples by ICP-MS. *Acta Petrologica. Sinica*, 2007, **23**(5), 1203–1210 (in Chinese).
25. Zou, C. N., Du, J. H., Xu, C. C., Wang, Z. C., Zhang, B. M., Wei, G. Q., Wang, T. S., Yao, G. S., Deng, S. H., Liu, J. J., Zhou, H., Xu, A. N., Yang, Z., Jiang, H., Gu, Z. D. Formation, distribution, resource potential and discovery of the Sinian-Cambrian giant gas field, Sichuan Basin, SW China. *Petroleum Exploration and Development*, 2014, **41**(3), 278–293 (in Chinese).
26. Yang, Y., Wen, L., Xie, J. R., Luo, B., Huang, P. H., Ran, Q., Zhou, G., Zhang, X. H., Wang, H., Tian, X. W., Zhang, Y., Chen, C. Progress and direction of marine carbonate gas exploration in Sichuan Basin. *China Petroleum Exploration*, 2020, **25**(3), 44–55 (in Chinese).
27. Taylor, S. R., McLennan, S. M. *The Continental Crust: Its Composition and Evolution: an Examination of the Geochemical Record Preserved in Sedimentary Rocks*. Science Press, Beijing, 1985.
28. Haskin, L. A., Haskin, M. A., Frey, F. A., Wildeman, T. R. Relative and absolute terrestrial abundances of the rare earths. In: *Origin and Distribution of the Elements* (Ahrens, L. H., ed.), International Series of Monographs in Earth Sciences, 1968, 889–912.
29. Fu, X., Wang, J., Zeng, Y., Tan, F., Feng, X. Trace elements in marine oil shale from the Changshe Mountain area, northern Tibet, China. *Energ. Source. Part A*, 2012, **34**(24), 2296–2306.
30. Patterson, J. H., Ramsden, A. R., Dale, L. S., Fardy, J. J. Geochemistry and mineralogical residences of trace elements in oil shales from Julia Creek, Queensland, Australia. *Chem. Geol.*, 1986, **55**(1–2), 1–16.
31. Garver, J. I., Royce, P. R., Smick, T. A. Chromium and nickel in shale of the Taconic foreland; a case study for the provenance of fine-grained sediments with an ultramafic source. *J. Sediment. Res.*, 1996, **66**(1), 100–106.
32. Paikaray, S., Banerjee, S., Mukherji, S. Geochemistry of shales from the Paleoproterozoic to Neoproterozoic Vindhyan Supergroup: Implications on provenance, tectonics and paleoweathering. *J. Asian Earth Sci*., 2008, **32**(1), 34–48.
33. Floyd, P. A., Leveridge, B. E. Tectonic environment of the Devonian Gramscatho

basin, south Cornwall: framework mode and geochemical evidence from turbiditic sandstones. *J. Geol. Soc.*, 1987, **144**(4), 531–542.

34. Ghosh, P., Bhattacharya, S. K., Dayal, A. M., Trivedi, J. R., Ebihara, M., Sarin, M. M., Chakrabarti, A. Trace element and isotopic studies of Permo-Carboniferous carbonate nodules from Talchir sediments of peninsular India: Environmental and provenance implications. *P. Indian AS - Earth*, 2002, **111**(2), 87–93.
35. Bhatia, M. R., Crook, K. A. W. Trace element characteristics of graywackes and tectonic setting discrimination of sedimentary basins. *Contrib. to Mineral. Petrol.*, 1986, **92**(2), 181–193.
36. Zhang, K. J. A Mediterranean-style model for early Neoproterozoic amalgamation of South China. *J. Geodyn.*, 2017, **105**, 1–10.
37. Kaufman, A. J., Jacobsen, S. B., Knoll, A. H. The vendian record of Sr and C isotopic variations in seawater: implications for tectonics and paleoclimate. *Earth Planet. Sci. Lett.*, 1993, **120**(3–4), 409–430.
38. Grotzinger, J. P., Bowring, S. A., Saylor, B. Z., Kaufman, A. J. Biostratigraphic and geochronologic constraints on early animal evolution. *Science*, 1995, **270**(5236), 598–604.
39. Knoll, A. H., Carroll, S. B. Early animal evolution: Emerging views from comparative biology and geology. *Science*, 1999, **284**(5423), 2129–2137.
40. Hayashi, K. I., Fujisawa, H., Holland, H. D., Ohmoto, H. Geochemistry of ~1.9 Ga sedimentary rocks from northeastern Labrador, Canada. *Geochim. Cosmochim. Acta*, 1997, **61**(19), 4115–4137.
41. McLennan, S. M., Hemming, S., McDaniel, D. K., Hanson, G. N. Geochemical approaches to sedimentation, provenance, and tectonics. In: *Processes Controlling the Composition of Clastic Sediments* (Johnsson, M. J., Basu, A., eds.), *Geol. Soc. Am. Spec. Pap.*, 1993, **284**, 21–40.
42. Roser, B. P., Korsch, R. J. Provenance signatures of sandstone-mudstone suites determined using discriminant function analysis of major-element data. *Chem. Geol.*, 1988, **67**(1–2), 119–139.
43. Allègre, C. J., Minster, J. F. Quantitative models of trace element behavior in magmatic processes. *Earth Planet. Sci. Lett.*, 1978, **38**(1), 1–25.
44. Fan, H., Wen, H., Zhu, X. Marine redox conditions in the Early Cambrian ocean: Insights from the Lower Cambrian phosphorite deposits, South China. *J. Earth Sci.*, 2016, **27**(2), 282–296.
45. Gao, P., Liu, G., Jia, C., Young, A., Wang, Z., Wang, T., Zhang, P., Wang, D. Redox variations and organic matter accumulation on the Yangtze carbonate platform during Late Ediacaran–Early Cambrian: Constraints from petrology and geochemistry. *Palaeogeogr. Palaeoclimatol. Palaeoecol.*, 2016, **450**, 91–110.
46. Guo, Q., Deng, Y., Hippler, D., Franz, G., Zhang, J. REE and trace element patterns from organic-rich rocks of the Ediacaran-Cambrian transitional interval. *Gondwana Res.*, 2016, **36**(1), 94–106.
47. Harnois, L. The CIW index: a new chemical index of weathering. *Sediment. Geol.*, 1988, **55**(3–4), 319–322.

48. Xu, Z., Lu, H., Zhao, C., Wang, X., Su, Z., Wang, Z., Liu, H., Wang, L., Lu, Q. Composition, origin and weathering process of surface sediment in Kumtagh Desert, Northwest China. *J. Geogr. Sci.*, 2011, **21**(6), 1062–1076.
49. Tobia, F. H., Mustafa, B. H. Geochemistry and mineralogy of the Al-rich shale from Baluti formation, Iraqi Kurdistan region: implications for weathering and provenance. *Arab. J. Geosci.*, 2016, **9**(20), 757.
50. Guo, L., Jia, C. C., Du, W. Geochemistry of Lower Silurian shale of Longmaxi Formation, southeastern Sichuan Basin, China: Implications for provenance and source weathering. *J. Cent. South Univ.*, 2016, **23**(3), 669–676.
51. Deng, T., Li, Y., Wang, Z., Yu, Q., Dong, S., Yan, L., Hu, W., Chen, B. Geochemical characteristics and organic matter enrichment mechanism of black shale in the Upper Triassic Xujiahe Formation in the Sichuan basin: Implications for paleoweathering, provenance and tectonic setting. *Mar. Petrol. Geol.,* 2019, **109**, 698–716.
52. Liu, S., Liu, B., Tang, S., Zhao, C., Tan, F., Xi, Z., Du, F. Palaeoenvironmental and tectonic controls on organic matter enrichment in the Middle Jurassic Dameigou Formation (Qaidam Basin, North China). *Palaeogeogr. Palaeoclimatol. Palaeoecol.*, 2022, **585**, 110747.
53. Liu, H., Wang, C., Li, Y., Deng, J., Deng, B., Feng, Y., Chen, H., Xu, Y., Zhao, S. Geochemistry of the black rock series of lower Cambrian Qiongzhusi Formation, SW Yangtze Block, China: Reconstruction of sedimentary and tectonic environments. *Open Geosci.*, 2021, **13**(1), 166–187.
54. Bai, Y., Liu, Z., Sun, P., Liu, R., Hu, X., Zhao, H., Xu, Y. Rare earth and major element geochemistry of Eocene fine-grained sediments in oil shale- and coal-bearing layers of the Meihe Basin, Northeast China. *J. Asian Earth Sci.*, 2015, **97**, Part A, 89–101.
55. Bai, Y., Lv, Q., Liu, Z., Sun, P., Xu, Y., Meng, J., Meng, Q., Xie, W., Wang, J., Wang, K. Major, trace and rare earth element geochemistry of coal and oil shale in the Yuqia area, Middle Jurassic Shimengou Formation, northern Qaidam Basin. *Oil Shale*, 2020, **37**(1), 1–31.
56. Dai, X., Du, Y., Ziegler, M., Wang, C., Ma, Q., Chai, R., Guo, H. Middle Triassic to Late Jurassic climate change on the northern margin of the South China Plate: Insights from chemical weathering indices and clay mineralogy. *Palaeogeogr. Palaeoclimatol. Palaeoecol.*, 2022, **585**, 110744.
57. Ofili, S., Soesoo, A. General geology and geochemistry of the Lokpanta Formation oil shale, Nigeria. *Oil Shale*, 2021, **38**(1), 1–25.
58. Ofili, S., Soesoo, A., Panova, E. G., Hints, R., Hade, S., Ainsaar, L. Geochemical reconstruction of the provenance, tectonic setting and paleoweathering of Lower Paleozoic black shales from Northern Europe. *Minerals*, 2022, **12**(5), 602.
59. McLennan, S. M. Weathering and global denudation. *J. Geol.*, 1993, **101**(2), 295–303.